

ON THE LONG TIME BEHAVIOR OF GAS FLOWS BY EVAPORATION FROM A PLANE CONDENSED PHASE

BY

SHIGERU TAKATA

Dedicated to Professor Yoshio Sone on his 70th birthday

Abstract

Evaporation from a plane condensed phase in the case of two species systems is studied on the basis of the kinetic theory of gases, with a special interest in the long time behavior of the mixture of vapors from initial equilibrium states. A standard finite-difference analysis by the use of the Garzó–Santos–Brey model Boltzmann equation is performed, and the long time behavior of the mixture and the condition for steady evaporation are clarified. Conventional gas-dynamic argument developed in [Y. Sone and H. Sugimoto, in *Adiabatic Waves in Liquid-Vapor Systems*, G.E.A. Meier and P.A. Thompson Eds., Springer, Berlin, 1990, pp. 293–304] is also applied, and the obtained numerical solutions are reported to be covered by the four-fold classification in this reference. It is, however, shown by the same argument that a certain class of the initial equilibrium states is not covered by that classification. The long time behavior of the mixture from this class of initial states is also discussed.

1. Introduction

Half-space problem of the Boltzmann equation for evaporation and/or condensation has been of great importance in the field of kinetic theory of

Received October 11, 2007.

AMS Subject Classification: 76P05, 76N15, 82B40, 82C40.

Key words and phrases: Kinetic theory of gases, Boltzmann equation, evaporation, binary mixture, vacuum, compressible flow.

gases (e.g., Refs. [1, 2, 3, 4, 5]).

From a physical or more specifically fluid-dynamic point of view, there is a strong motivation to study the problem: the solution of the problem provides the fluid-dynamic equation with the information about the appropriate boundary condition for gas flows at the interface with its condensed phase [6, 7, 8]. A little more specifically, it is known that steady evaporation and/or condensation may occur only conditionally and it is this condition that plays the part of the boundary condition at the interface in fluid dynamics.

One of the interesting aspects of the problem is a dramatic change of the condition at the reverse point (between evaporation and condensation) and at the sonic point of the induced flow.¹ For instance, steady evaporation may occur only subsonically and perpendicularly to the interface, and there is only one parameter that can be chosen freely among the three (pressure, temperature, and Mach number) that specify the state of gas at a far field. On the other hand, steady condensation may occur subsonically and supersonically and not always perpendicularly; one can choose the parameters at a far field (pressure, temperature, and Mach numbers in perpendicular and tangential directions) freely except one for subsonic case, while one can do it freely within a certain condition (more specifically satisfying a certain inequality) for supersonic case. These interesting features have been clarified by intensive numerical analyses [9, 10, 11, 12] (see also the references in Ref. [2]). It should be mentioned, however, that the abrupt change of the condition at the reverse point was first clarified by an asymptotic analysis by Sone [13] and that his analysis was later developed to achieve a comprehensive understanding of the changes not only at the reverse point but also at the sonic point for condensation [14, 3, 5]. Thus fascinating structure of the steady solutions of the half space problem has also been attracting the researchers in mathematics, and rigorous mathematical theories have also been developing (see, e.g., Refs. [15, 16, 17, 18] and the references therein).

In the present paper, we consider the half-space problem for evaporation in two species systems. We follow the strategy of Sone and Sugimoto [10]. That is, we numerically study the time-development of the behavior of the gas mixture in the half space from initial equilibrium states, especially its long-time behavior and the condition of the steady evaporation. We do

¹Here and hereinafter, the “sonic” means that the flow component normal to the interface is sonic. The tangential component is always excluded in this context.

not expect a qualitative difference from the single species case, but rather expect to have a straightforward extension, as our previous contributions in the linear [19, 20] and weakly nonlinear [21, 22] regimes suggested. In fact, the results of our numerical computations to be presented in this paper support our expectation. However, we shall point out that the long time behavior of the mixture from a certain class of initial states is not covered by the four-fold classification in Ref. [10]. The classification was induced in this reference from the results of intensive numerical analyses by the use of the conventional gas-dynamic relations and the condition for steady evaporation. One additional category, which is naturally deduced from the physical picture of one of the four categories, is needed to complete the classification. This is not peculiar to two species systems, but is also true for single species systems. Although our result does not influence the main conclusions of Ref. [10], we report it with detail descriptions of the above conventional gas-dynamic argument.

The paper is organized as follows. After the statement of the problem in Section 2, we first make a brief summary of the existing results for single species systems in Section 3. Then, in the same section, we report the results of our numerical computations by a standard finite-difference method on the basis of the Garzó–Santos–Brey model Boltzmann equation [23] for gas mixtures. Next, in Section 4.1. we provide detailed description of the way of recovery of the long time behavior from a given initial state by the use of the conventional gas dynamics (the Euler set of equations) and of the condition for steady evaporation presented in Section 3. It is essentially a simple application of the procedure in Sone and Sugimoto [10] to the case of two species systems, but we point out that there is a region of parameter that is not covered by the four-fold classification induced from the numerical analyses performed in this reference and in the present work. In Section 4.2, we present a picture of the long time behavior expected by the continuation of the above procedure, which results in the appearance of a vacuum region propagating toward the undisturbed far field. Finally, we conclude the paper in Section 5.

2. Statement of the Problem

Consider a semi-infinite expanse of a binary mixture of vapors, species A and B, bounded by a planar interface with its condensed phase, i.e., the liquid mixture of the same species. The interface does not move in time and

is located at $X_1 = 0$, where X_i is the Cartesian coordinates of the physical space. The temperature T_w and chemical composition of the condensed phase are uniform and constant. At time $t = 0$, the mixture is in a uniform equilibrium state with pressure p_0 , temperature T_0 , concentration χ_0^A of species A, and flow velocity $(u_0, 0, 0)$. For $t > 0$, because of the interaction with the condensed phase, the state of the vapor mixture is disturbed from the initial equilibrium state and the disturbance propagates in the half-space toward the far field. We will study the time development of the disturbance on the basis of kinetic theory of gases, especially its long time behavior. We are interested in the case when evaporation from the condensed phase takes place.

In the analysis, we assume that the vapor molecules impinging on the condensed phase are absorbed completely and the vapor molecules leaving there obey the half-range resting Maxwellian with the pressure p_w , concentration χ_w^A of species A, and temperature T_w , where χ_w^A and p_w denote the concentration of species A and the pressure in the mixture that is in equilibrium with the condensed phase with constant temperature T_w and chemical composition. We treat respective species as a monatomic gas.

3. Long Time Behavior and Condition for Steady Evaporation: Numerical Evidence

The corresponding problem for a single species system, or the present problem in the case of $\chi_0^A = \chi_w^A = 1$, has been studied intensively on the basis of the BKW (or BGK) equation [24, 25] by Sone and Sugimoto [10], where many details of the time development of disturbance were clarified mainly numerically by the finite-difference method (see also Chap. 6 of Ref. [5]). Among those details, we list here two main outcomes of this reference having a direct relation to the discussions in the present paper:

1. On the long time behavior: Four types of behavior were observed numerically.
 - (a) Disturbance propagates as a shock wave followed by a contact layer. The Knudsen layer is established in the vicinity of the interface with the condensed phase. New uniform (and constant) states appear both between the shock wave and the contact layer and between the contact layer and the Knudsen layer. We refer this case as type I.

- (b) Disturbance propagates as an expansion wave followed by a contact layer. The Knudsen layer is established in the vicinity of the interface. New uniform (and constant) states appear both between the expansion wave and the contact layer and between the contact layer and the Knudsen layer. We refer this case as type II.
- (c) As type I, disturbance propagates as a shock wave followed by a contact layer. But behind the contact layer, there appears an expansion wave propagating toward the interface relative to the flow of the mixture. The Knudsen layer whose tail is a sonic state is established in the vicinity of the interface. The sonic state is also the upstream of the expansion wave, so that the front of the expansion wave does not move relative to the interface. New uniform (and constant) states appear both between the shock wave and the contact layer and between the contact layer and the expansion wave. We refer this case as type III.
- (d) As type II, disturbance propagates as an expansion wave followed by a contact layer. But behind the contact layer, as type III, there appears another expansion wave propagating toward the interface relative to the flow of the mixture. The Knudsen layer whose tail is a sonic state is established in the vicinity of the interface. The sonic state is also the upstream of the latter expansion wave, so that its front does not move relative to the interface. New uniform (and constant) states appear both between the former expansion wave and the contact layer and between the contact layer and the latter expansion wave. We refer this case as type IV.

Here, the contact layer corresponds to the contact discontinuity in the conventional gas dynamics. Henceforth, following Ref. [10], we refer the expansion wave propagating toward the undisturbed far field as “expansion wave R” and that propagating toward the interface relative to the flow as “expansion wave L.” For instance, the expansion wave R appears in type II, the expansion wave L in type III, and both the expansion waves R and L in type IV.

2. On the steady evaporation:

- (a) Supersonic evaporating flow does not occur.
- (b) Evaporating flow occurs always perpendicularly to the interface with the condensed phase. This statement requires supplemental results of Ref. [12].

- (c) Behind the Knudsen layer, a uniform equilibrium state is established. Denoting by p_* , T_* , and $(u_*, 0, 0)$ the pressure, temperature, and flow velocity in the state, the ratios of pressure p_*/p_w and of temperature T_*/T_w are determined by the Mach number M_* of the flow, i.e.,

$$\frac{p_*}{p_w} = h_1(M_*), \quad \frac{T_*}{T_w} = h_2(M_*), \quad 0 \leq M_* \leq 1, \quad (1)$$

where $M_* = u_*/\sqrt{\gamma RT_*}$ with $\gamma = 5/3$ and R is the specific gas constant defined by $R = k/m$, the Boltzmann constant k divided by the mass of a molecule m .

Further, from these results, which type of long time behavior occurs from the given initial state was derived in Ref. [10] by the use of the conventional gas-dynamic relations [26, 27, 28] on shock wave, simple wave, and contact discontinuity.

Following the strategy of Ref. [10], the author, with the help of Mr. Imoto, recently carried out numerical computations for the problem stated in Section 2 on the basis of the Garzó–Santos–Brey model Boltzmann equation for gas mixtures [23] (GSB model, for short) [H. Imoto, Master Thesis, Graduate School of Engineering, Kyoto University, 2006 (in Japanese)]. We observed that our numerical solutions were covered by the four-fold classification into types I–IV. Typical examples are shown in Figs. 1–4,² where M_0 is the Mach number of the flow at the initial undisturbed state:

$$M_0 = \frac{u_0}{a_0} \quad \text{with} \quad a_0 = \sqrt{\gamma R_0 T_0}.$$

Here a_0 is the sound speed in the initial undisturbed state, $R_0 = k/m_0$, and $m_0 = m^A \chi_0^A + m^B (1 - \chi_0^A)$. (R_0 is the specific gas constant based on the average molecular mass m_0 at the initial undisturbed state.) We also obtained, as in the single-species case, the steady solution for subsonic evaporation. Denoting by p_* , χ_*^A , T_* , and $(u_*, 0, 0)$ the pressure, concentration,

²In the case of the GSB model, the collision frequency of a molecule of species α for the collision with species β of number density n^β is given by $K^{\alpha\beta} n^\beta$, where α and β denote A or B and $K^{\alpha\beta}$ is a constant depending on α and β . Numerical results presented in this paper are those for the case that $K^{\alpha\beta}$ is a common constant C , i.e., $K^{AA} = K^{AB} = K^{BA} = K^{BB} = C$. The reference collision frequency ν_w^A in Figures 1–4 is expressed, with this C , as $\nu_w^A = C (\chi_w^A p_w / k T_w)$.

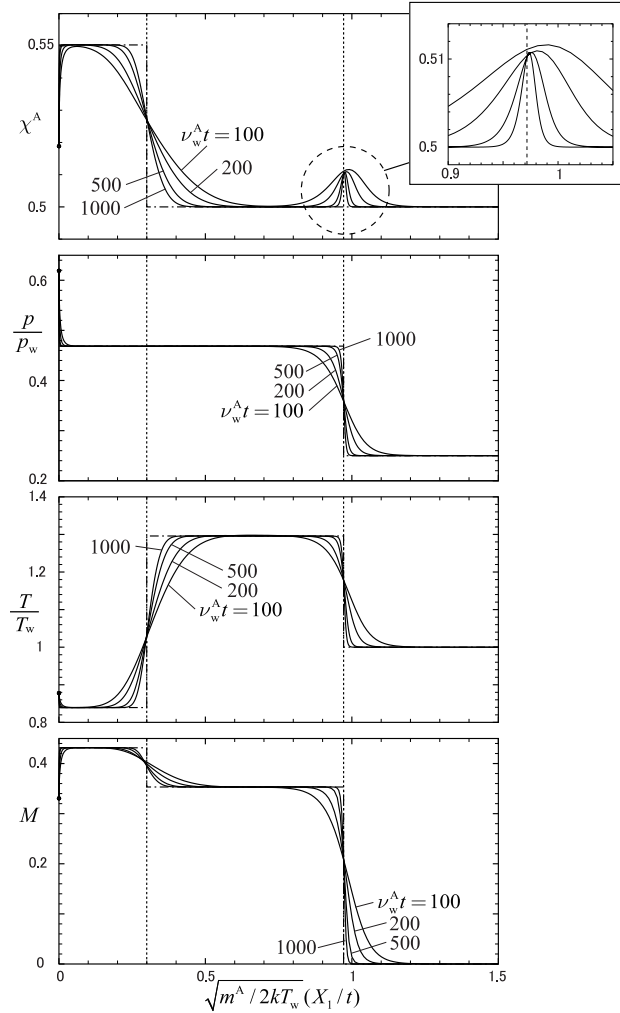


Figure 1. Time development of the solution of the GSB model in the case of $m^B/m^A = 2$, $\chi_w^A = \chi_0^A = 0.5$, $T_0/T_w = 1$, $p_0/p_w = 0.25$, and $M_0 = 0$: type I. From the top, the local concentration χ^A of species A, pressure p , temperature T , and Mach number M are shown as a function of X_1/t for $\nu_w^A t = 100, 200, 500$, and 1000 , where ν_w^A is the reference collision frequency of a molecule for the collision with species A of the number density $p_w \chi_w^A / kT_w$. Small circle on the vertical axis indicates the value at $X_1/t = 0$. Dash-dot line indicates the asymptotic profile predicted by the conventional gas dynamics with the aid of relation (2) [or (3)] (see Section 4.1). Dashed line indicates the predicted position of the contact discontinuity and the shock wave in the X_1/t coordinate.

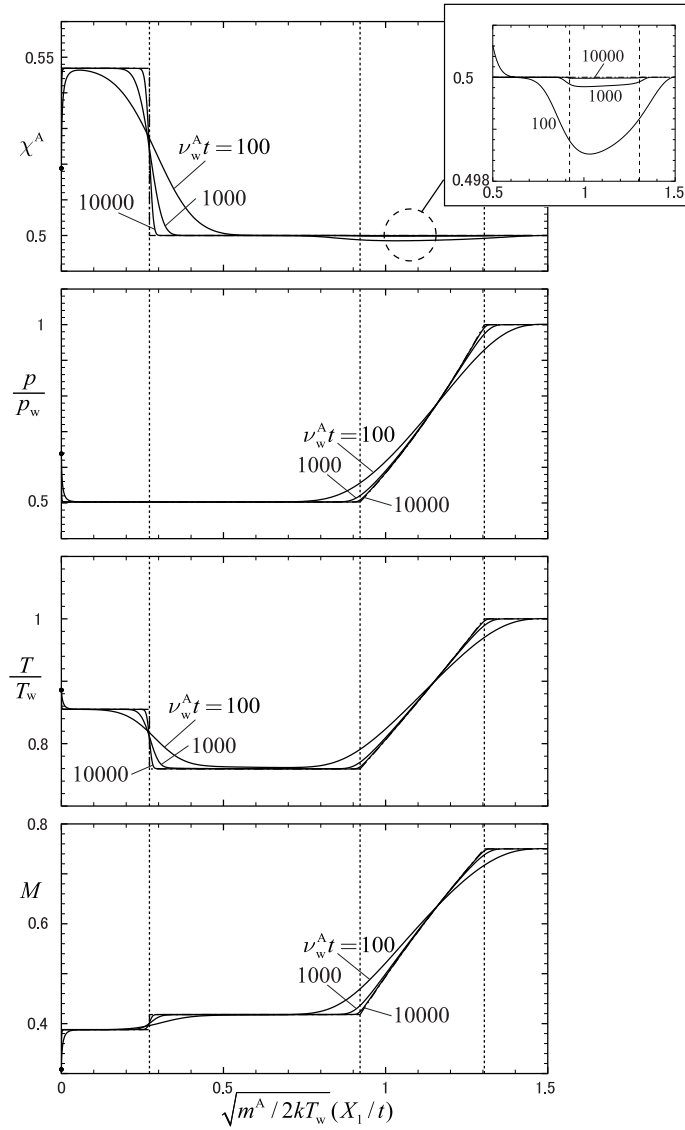


Figure 2. Time development of the solution of the GSB model in the case of $m^B/m^A = 2$, $\chi_w^A = \chi_0^A = 0.5$, $T_0/T_w = 1$, $p_0/p_w = 1$, and $M_0 = 0.75$: type II. From the top, the local concentration χ^A of species A, pressure p , temperature T , and Mach number M are shown as a function of X_1/t for $\nu_w^A t = 100, 1000$, and 10000 . See also the caption of Figure 1. Dashed line indicates the position of the contact discontinuity and the front and tail of the expansion wave R in the X_1/t coordinate.

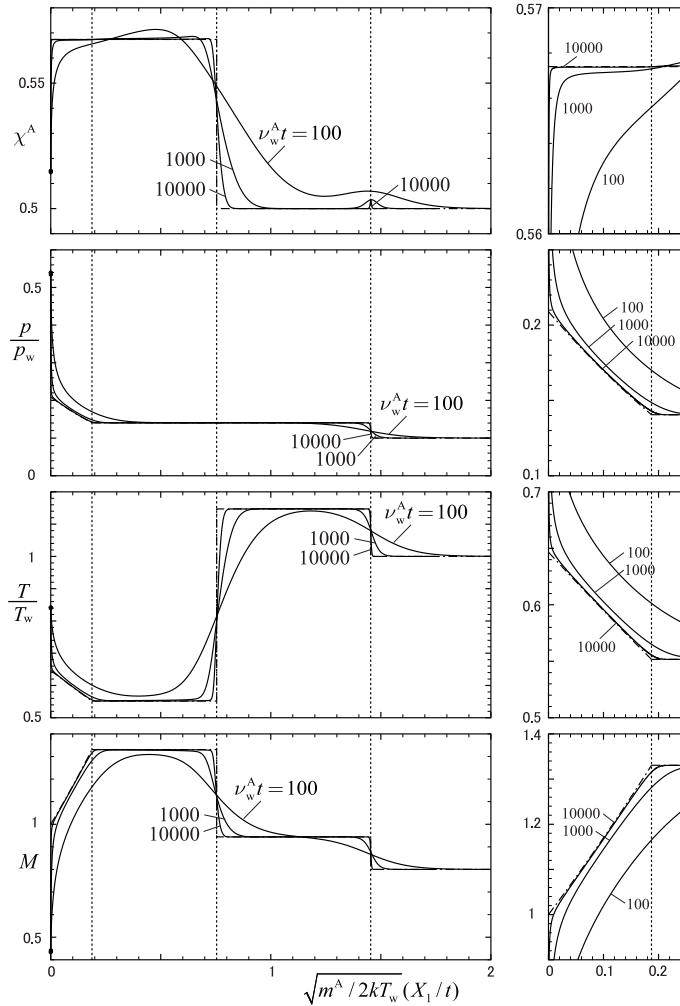


Figure 3. Time development of the solution of the GSB model in the case of $m^B/m^A = 2$, $\chi_w^A = \chi_0^A = 0.5$, $T_0/T_w = 1$, $p_0/p_w = 0.1$, and $M_0 = 0.8$: type III. From the top, the local concentration χ^A of species A, pressure p , temperature T , and Mach number M are shown as a function of X_1/t for $\nu_w^A t = 100, 1000$, and 10000 . See also the caption of Figure 1. Dashed line indicates the position of the tail of the expansion wave L, the contact discontinuity, and the shock wave in the X_1/t coordinate. Narrow figure on the right is a close up of the part corresponding to the Knudsen layer and expansion wave L.

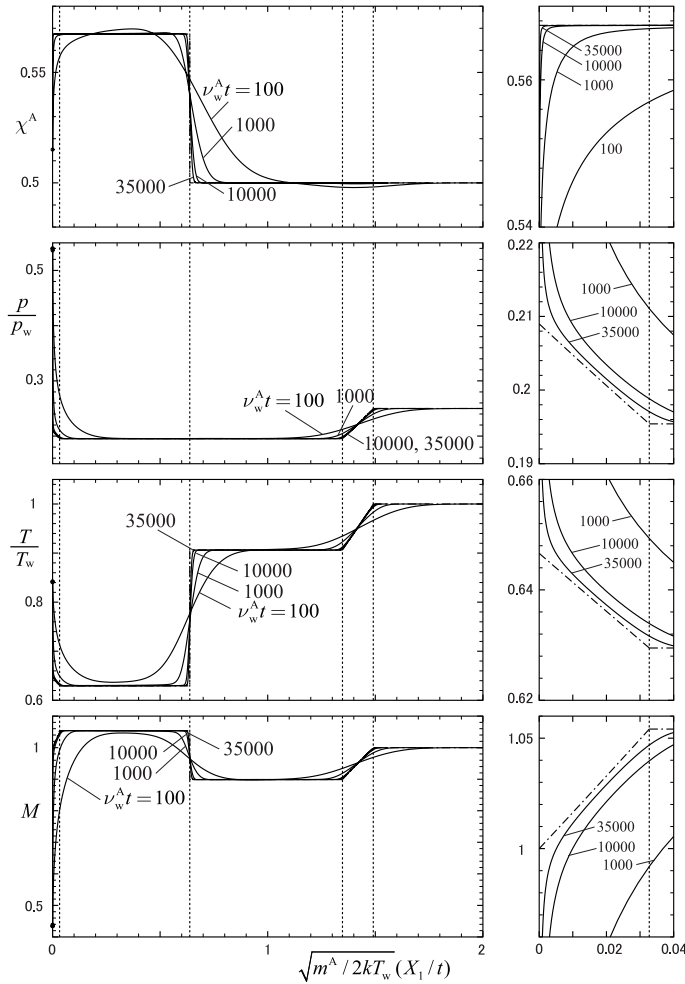


Figure 4. Time development of the solution of the GSB model in the case of $m^B/m^A = 2$, $\chi_w^A = \chi_0^A = 0.5$, $T_0/T_w = 1$, $p_0/p_w = 0.25$, and $M_0 = 1$: type IV. From the top, the local concentration χ^A of species A, pressure p , temperature T , and Mach number M are shown as a function of X_1/t for $\nu_w^A t = 100, 1000, 10000$, and 35000 . See also the caption of Figure 1. Dashed line indicates the position of the tail of the expansion wave L, the contact discontinuity, and the tail and front of the expansion wave R in the X_1/t coordinate. Narrow figure on the right is a close up of the part corresponding to the Knudsen layer and expansion wave L.

temperature, and flow velocity at the uniform equilibrium state behind the Knudsen layer, the ratios of pressure p_*/p_w , of concentration χ_*^A/χ_w^A , and of temperature T_*/T_w are determined by the Mach number M_* of the flow, i.e.,

$$\frac{p_*}{p_w} = h_p(M_*; \chi_w^A), \quad \frac{T_*}{T_w} = h_T(M_*; \chi_w^A), \quad \frac{\chi_*^A}{\chi_w^A} = h_\chi(M_*; \chi_w^A), \quad (2)$$

with $0 \leq M_* \leq 1$. Here $M_* = u_*/a_*$ with a_* being the sound speed defined by $a_* = \sqrt{\gamma R_* T_*}$, where $R_* = k/[m^A \chi_*^A + m^B(1 - \chi_*^A)]$. The functions h_p , h_T , and h_χ in the case of the GSB model are shown in Figure 5 (see Ref. [22] for $M_* \ll 1$ for more general molecular interactions). In the figure, the DSMC results by Frezzotti [29] for a mixture of hard sphere gases with a common molecular diameter are also shown. As is seen from the figure, h_p and h_T are positive, take the value of unity at $M_* = 0$, and monotonically decrease as M_* increases. These properties are the same as those of h_1 and h_2 in Ref. [10] for single species gases. The function h_χ is also positive, takes the value of unity at $M_* = 0$, and is monotonic with respect to M_* . However, increasing or decreasing depends on the mass ratio m^B/m^A , i.e., h_χ is increasing if $m^B/m^A > 1$ and decreasing if $m^B/m^A < 1$. This motivates us to use another function $h_u(M_*; \chi_w^A)$, in place of $h_\chi(M_*; \chi_w^A)$, defined by

$$h_u(M_*; \chi_w^A) = \frac{u_*}{a_w} = M_* \frac{a_*}{a_w}.$$

Here $a_w = \sqrt{\gamma R_w T_w}$ and R_w is the specific gas constant defined by $R_w = k/[m^A \chi_w^A + m^B(1 - \chi_w^A)]$. The function h_u is related to h_χ through a_* as

$$h_u(M_*; \chi_w^A) = M_* \sqrt{\frac{[(m^A - m^B)\chi_w^A + m^B]h_T(M_*; \chi_w^A)}{(m^A - m^B)\chi_w^A h_\chi(M_*; \chi_w^A) + m^B}}.$$

The function h_u is shown in the bottom right panel of Figure 5. It takes the value of zero at $M_* = 0$ and increases monotonically with M_* , irrespective of the value of the mass ratio m^B/m^A . In the rest of the paper, we mainly use the set of relations

$$\left. \begin{aligned} \frac{p_*}{p_w} &= h_p(M_*; \chi_w^A), & \frac{T_*}{T_w} &= h_T(M_*; \chi_w^A), \\ \frac{u_*}{a_w} &= h_u(M_*; \chi_w^A), \end{aligned} \right\} \quad 0 \leq M_* \leq 1, \quad (3)$$

in place of (2). The numerical data of the functions h_p , h_T and h_u are tabulated in Tables 1–3.

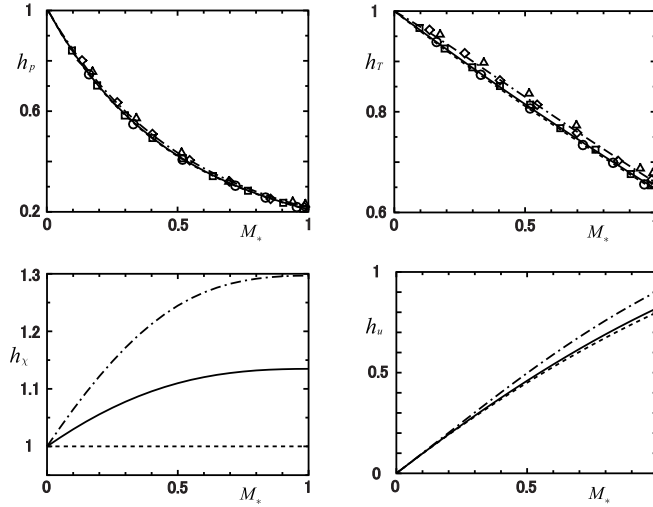


Figure 5. Functions h_p , h_T , h_χ , and h_u in the case of $\chi_w^A = 0.5$. Dashed line ($m^B/m^A = 1$), solid line ($m^B/m^A = 2$), and dash-dot line ($m^B/m^A = 5$) indicate the present results for the GSB model. Symbols \circ ($m^B/m^A = 1$), \square ($m^B/m^A = 2$), \diamond ($m^B/m^A = 5$), and \triangle ($m^B/m^A = 10$) indicate the DSMC results taken from Figure 5 in Ref. [29] for a mixture of hard sphere gases with a common molecular diameter.

Table 1. Function h_p (GSB model). In the case of $m^B/m^A = 1$, h_p is independent of χ_w^A and is identical to h_1 for the BKW (or BGK) model in Ref. [5]. See the footnote 2.

$M_* \setminus \chi_w^A$	$m^B/m^A = 1$			$m^B/m^A = 2$			$m^B/m^A = 5$			
	—	0.2	0.5	0.8	0.2	0.5	0.8	0.2	0.5	0.8
0.00	1.0000	1.0000	1.0000	1.0000	1.0000	1.0000	1.0000	1.0000	1.0000	1.0000
0.05	0.9083	0.9090	0.9095	0.9092	0.9110	0.9141	0.9141	0.9110	0.9141	0.9141
0.10	0.8267	0.8279	0.8288	0.8283	0.8315	0.8367	0.8362	0.8315	0.8367	0.8362
0.15	0.7540	0.7555	0.7566	0.7560	0.7603	0.7668	0.7657	0.7603	0.7668	0.7657
0.20	0.6891	0.6908	0.6920	0.6912	0.6964	0.7036	0.7018	0.6964	0.7036	0.7018
0.25	0.6310	0.6328	0.6341	0.6332	0.6389	0.6465	0.6440	0.6389	0.6465	0.6440
0.30	0.5789	0.5807	0.5820	0.5811	0.5872	0.5947	0.5917	0.5872	0.5947	0.5917
0.35	0.5321	0.5339	0.5352	0.5343	0.5405	0.5478	0.5444	0.5405	0.5478	0.5444
0.40	0.4900	0.4918	0.4930	0.4921	0.4983	0.5053	0.5016	0.4983	0.5053	0.5016
0.45	0.4520	0.4538	0.4549	0.4540	0.4602	0.4667	0.4629	0.4602	0.4667	0.4629
0.50	0.4177	0.4194	0.4205	0.4196	0.4256	0.4317	0.4279	0.4256	0.4317	0.4279
0.55	0.3867	0.3883	0.3893	0.3884	0.3943	0.3999	0.3962	0.3943	0.3999	0.3962
0.60	0.3586	0.3601	0.3610	0.3602	0.3658	0.3710	0.3674	0.3658	0.3710	0.3674
0.65	0.3331	0.3345	0.3353	0.3346	0.3399	0.3448	0.3413	0.3399	0.3448	0.3413
0.70	0.3099	0.3112	0.3120	0.3113	0.3163	0.3208	0.3175	0.3163	0.3208	0.3175
0.75	0.2887	0.2900	0.2907	0.2900	0.2948	0.2990	0.2958	0.2948	0.2990	0.2958
0.80	0.2695	0.2706	0.2713	0.2707	0.2752	0.2791	0.2761	0.2752	0.2791	0.2761
0.85	0.2519	0.2529	0.2536	0.2530	0.2573	0.2608	0.2581	0.2573	0.2608	0.2581
0.90	0.2358	0.2368	0.2374	0.2368	0.2408	0.2442	0.2416	0.2408	0.2442	0.2416
0.95	0.2210	0.2220	0.2225	0.2220	0.2258	0.2289	0.2265	0.2258	0.2289	0.2265
1.00	0.2076	0.2084	0.2090	0.2086	0.2120	0.2151	0.2129	0.2120	0.2151	0.2129

Table 2. Function h_T (GSB model). In the case of $m^B/m^A = 1$, h_T is independent of χ_w^A and is identical to h_2 for the BKW (or BGK) model in Ref. [5]. See the footnote 2.

$M_* \setminus \chi_w^A$	$m^B/m^A = 1$	$m^B/m^A = 2$			$m^B/m^A = 5$		
	—	0.2	0.5	0.8	0.2	0.5	0.8
0.00	1.0000	1.0000	1.0000	1.0000	1.0000	1.0000	1.0000
0.05	0.9798	0.9805	0.9809	0.9805	0.9833	0.9847	0.9833
0.10	0.9600	0.9612	0.9618	0.9612	0.9660	0.9687	0.9660
0.15	0.9404	0.9420	0.9429	0.9420	0.9484	0.9520	0.9484
0.20	0.9212	0.9231	0.9241	0.9230	0.9305	0.9350	0.9304
0.25	0.9022	0.9043	0.9054	0.9043	0.9127	0.9176	0.9122
0.30	0.8835	0.8858	0.8870	0.8857	0.8949	0.9001	0.8940
0.35	0.8651	0.8675	0.8687	0.8674	0.8771	0.8825	0.8759
0.40	0.8470	0.8494	0.8507	0.8493	0.8594	0.8648	0.8578
0.45	0.8290	0.8315	0.8328	0.8313	0.8419	0.8472	0.8399
0.50	0.8113	0.8139	0.8151	0.8136	0.8244	0.8296	0.8221
0.55	0.7938	0.7964	0.7976	0.7961	0.8070	0.8121	0.8045
0.60	0.7765	0.7790	0.7802	0.7788	0.7897	0.7946	0.7871
0.65	0.7594	0.7619	0.7630	0.7616	0.7726	0.7773	0.7698
0.70	0.7424	0.7448	0.7460	0.7446	0.7555	0.7600	0.7526
0.75	0.7255	0.7280	0.7291	0.7277	0.7385	0.7429	0.7356
0.80	0.7088	0.7112	0.7123	0.7109	0.7215	0.7259	0.7187
0.85	0.6923	0.6946	0.6957	0.6943	0.7047	0.7089	0.7019
0.90	0.6758	0.6781	0.6791	0.6778	0.6880	0.6921	0.6853
0.95	0.6595	0.6617	0.6628	0.6615	0.6715	0.6754	0.6688
1.00	0.6435	0.6455	0.6466	0.6455	0.6550	0.6591	0.6528

Table 3. Function h_u (GSB model). In the case of $m^B/m^A = 1$, h_u is identical to $M_*\sqrt{h_T}$ and thus is not shown in the table [see the equation just before (3)].

$M_* \setminus \chi_w^A$	$m^B/m^A = 2$			$m^B/m^A = 5$		
	0.2	0.5	0.8	0.2	0.5	0.8
0.00	0.0000	0.0000	0.0000	0.0000	0.0000	0.0000
0.05	0.0496	0.0496	0.0496	0.0498	0.0502	0.0503
0.10	0.0983	0.0986	0.0985	0.0991	0.1006	0.1011
0.15	0.1461	0.1467	0.1465	0.1480	0.1512	0.1522
0.20	0.1931	0.1941	0.1937	0.1962	0.2018	0.2033
0.25	0.2391	0.2406	0.2400	0.2439	0.2522	0.2541
0.30	0.2843	0.2863	0.2854	0.2909	0.3024	0.3045
0.35	0.3285	0.3311	0.3299	0.3373	0.3523	0.3542
0.40	0.3718	0.3750	0.3735	0.3830	0.4015	0.4031
0.45	0.4141	0.4179	0.4161	0.4278	0.4501	0.4511
0.50	0.4555	0.4599	0.4577	0.4719	0.4978	0.4980
0.55	0.4960	0.5009	0.4984	0.5151	0.5445	0.5437
0.60	0.5354	0.5409	0.5380	0.5573	0.5901	0.5882
0.65	0.5739	0.5799	0.5766	0.5984	0.6344	0.6315
0.70	0.6113	0.6179	0.6143	0.6385	0.6774	0.6735
0.75	0.6477	0.6548	0.6508	0.6774	0.7191	0.7142
0.80	0.6830	0.6905	0.6863	0.7151	0.7593	0.7537
0.85	0.7173	0.7252	0.7207	0.7515	0.7982	0.7919
0.90	0.7505	0.7588	0.7540	0.7867	0.8356	0.8288
0.95	0.7826	0.7914	0.7863	0.8206	0.8717	0.8644
1.00	0.8137	0.8228	0.8176	0.8533	0.9065	0.8989

In closing this section, we introduce for later convenience the subscript s in order to denote the quantities at the state of steady sonic evaporation:

$$\left. \begin{aligned} \frac{p_{*s}}{p_w^A} &= h_p(1; \chi_w^A), & \frac{T_{*s}}{T_w} &= h_T(1; \chi_w^A), \\ \frac{\chi_{*s}^A}{\chi_w^A} &= h_\chi(1; \chi_w^A), & \frac{u_{*s}}{a_w} &= h_u(1; \chi_w^A), \\ R_{*s} &= \frac{k}{\chi_{*s}^A m^A + (1 - \chi_{*s}^A) m^B}. \end{aligned} \right\} \quad (4)$$

Note that u_{*s} is identical to the sound speed a_{*s} defined by $a_{*s} = \sqrt{\gamma R_{*s} T_{*s}}$.

4. Recovery of the Long Time Behavior by the Conventional Gas Dynamics

In the present section, we shall take on faith that the relation (3) for the steady evaporation and the basic property of h_p , h_T , and h_u are true in general. In Section 4.1, we derive the region of parameters where the above four types of long time behavior are observed by using the conventional gas-dynamic relations on shock wave, simple wave, and contact discontinuity. We also describe the way to recover the long time behavior by conventional gas dynamics. Through the analyses in Section 4.1, it will become clear that the region of parameters for evaporation is not entirely covered with the four categories: types I–IV. In Section 4.2, we present such a new category of the long time behavior that covers the remaining region.

4.1. Parameter range of the four categories

In the present subsection, we consider the range of parameters where each type of long time behavior, type I–IV, should be observed. We also describe how to recover the long time behavior by the conventional gas dynamics.

Among Sections 4.1.1–4.1.4 below, Section 4.1.4 contains the most important result, because it shows that the four-fold classification of evaporation into types I–IV is not complete even in the case of single species systems.

We start with making the following conjecture on the property of the functions h_p , h_T , and h_u :

Conjecture 1. *The functions $h_p(M_*; \chi_w^A)$ and $h_T(M_*; \chi_w^A)$ are monotonically decreasing functions of M_* in $0 \leq M_* \leq 1$, and they take the*

value of unity at $M_* = 0$, i.e., $h_p(0; \chi_w^A) = 1$ and $h_T(0; \chi_w^A) = 1$. On the other hand, $h_u(M_*; \chi_w^A)$ is a monotonically increasing function of M_* in $0 \leq M_* \leq 1$, and it takes the value of zero at $M_* = 0$, i.e., $h_u(0; \chi_w^A) = 0$.

4.1.1. Parameter range of type I

The behavior of type I is schematically shown in Figure 6, where US is the abbreviation of the (constant) uniform state. Henceforth, the abbreviations KL, CL, and SW are also used to denote the Knudsen layer, contact layer, and shock wave, respectively. The subscripts + and – are added to US in order to denote the upstream and downstream uniform states of the contact layer. As shown in the figure, the half space is divided, according to the local state of the mixture, into six parts as

$$(KL)+(US_-)+(CL)+(US_+)+(SW)+(undisturbed\ US),$$

where the order of each part corresponds to the position from the interface with the condensed phase.

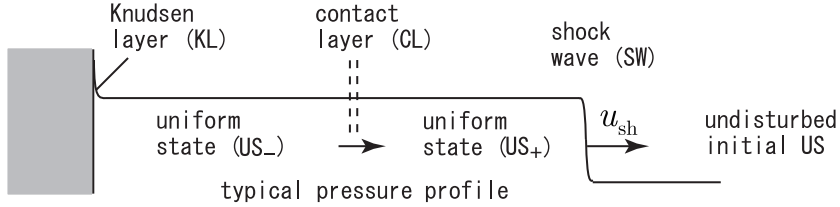


Figure 6. Schematic of the behavior of mixture: type I.

Let us denote the pressure, concentration, temperature, and flow velocity in the US_{\pm} by p_{\pm} , χ_{\pm}^A , T_{\pm} , and $(u_{\pm}, 0, 0)$. The shock relation, the Rankine–Hugoniot relation for non-reacting monotonic ideal gas mixtures, relates the sets of parameters between the US_+ and the undisturbed US as

$$\frac{p_+}{p_0} = 1 + \frac{2\gamma}{\gamma+1}(M^2 - 1), \quad \frac{T_+}{T_0} = 1 + \frac{2(\gamma-1)\gamma M^2 + 1}{(\gamma+1)^2 M^2}(M^2 - 1), \quad (5a)$$

$$\frac{\chi_+^A}{\chi_0^A} = 1, \quad \frac{u_{sh} - u_0}{u_{sh} - u_+} = \frac{(\gamma+1)M^2}{(\gamma-1)M^2 + 2}, \quad M = \frac{u_{sh} - u_0}{a_0}, \quad (5b)$$

where $(u_{sh}, 0, 0)$ is the velocity of the shock wave. In addition, across the contact discontinuity, the pressure and flow velocity are both continuous,

i.e.,

$$p_+ = p_-, \quad u_+ = u_-. \quad (6)$$

In the present situation, the inequalities

$$u_+ \geq \max(0, u_0), \quad \mathcal{M} \geq 1, \quad (7)$$

must be satisfied. The former is required because the shock wave moves toward the far field. The latter is a consequence of the second law of thermodynamics, i.e., the entropy condition across the shock wave. Since the Knudsen layer connects the interface to the US₋, the quantities with subscript * in (3) are identical to those in US₋, i.e.,

$$\left. \begin{aligned} \frac{p_-}{p_w} &= h_p(M_-; \chi_w^A), & \frac{T_-}{T_w} &= h_T(M_-; \chi_w^A), \\ \frac{u_-}{a_w} &= h_u(M_-; \chi_w^A), \end{aligned} \right\} 0 \leq M_- \leq 1, \quad (8)$$

where M_- is defined by $M_- = u_-/a_-$ with $a_- = \sqrt{\gamma R_- T_-}$ and $R_- = k/[m^A \chi_-^A + m^B(1 - \chi_-^A)]$. Needless to say, a_- is the sound speed in the US₋.

Now, we fix the values of T_0/T_w and χ_0^A and derive the region in the M_0 - p_0/p_w plane where the type I be observed (region I, for short). For this purpose, we first eliminate u_{sh} from the second equation of (5b) by the use of the third equation of (5b) to have

$$u_0 = u_+ - \frac{2(\mathcal{M}^2 - 1)}{(\gamma + 1)\mathcal{M}} a_0. \quad (9)$$

It is seen from (9) that the first inequality in (7) is included in the condition $\mathcal{M} \geq 1$. With keeping this in mind and taking into account the relation (6) across the contact layer, we obtain a two-parameter representation of region I in terms of \mathcal{M} and M_- from the first equations of (5a) and (8), the last equation of (8), and (9):

$$\left. \begin{aligned} \frac{p_0}{p_w} &= \frac{h_p(M_-; \chi_w^A)}{1 + \frac{2\gamma}{\gamma+1}(\mathcal{M}^2 - 1)}, \\ M_0 &= \frac{a_w}{a_0} h_u(M_-; \chi_w^A) - \frac{2(\mathcal{M}^2 - 1)}{(\gamma+1)\mathcal{M}}, \end{aligned} \right\} \mathcal{M} \geq 1, \quad 0 \leq M_- \leq 1. \quad (10)$$

The region I is shown in Figure 7, in which the isolines of M_- (or \mathcal{M}) are also drawn. It is seen from (10) that, as M_0 increases, p_0/p_w decreases monotonically along the isoline of \mathcal{M} but increases monotonically along the isoline of M_- because of the Conjecture 1. Therefore, the correspondence between

$(M_0, p_0/p_w)$ and (\mathcal{M}, M_-) is one-to-one, and region I has the following three boundary curves expressed as extreme cases of (10):

Curve A

$$\frac{p_0}{p_w} = h_p(M_-; \chi_w^A), \quad M_0 = \frac{a_w}{a_0} h_u(M_-; \chi_w^A), \quad 0 \leq M_- \leq 1, \quad (11)$$

which is obtained by letting $\mathcal{M} = 1$ in (10). This curve connects the points X and Y in Figure 7.

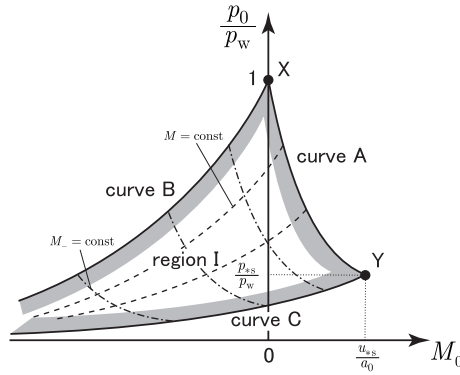


Figure 7. Schematic of region I in the M_0 - p_0/p_w plane.

Curve B

$$\frac{p_0}{p_w} = \frac{1}{1 + \frac{2\gamma}{\gamma+1}(\mathcal{M}^2 - 1)}, \quad M_0 = -\frac{2(\mathcal{M}^2 - 1)}{(\gamma + 1)\mathcal{M}}, \quad \mathcal{M} \geq 1, \quad (12)$$

which is obtained by letting $M_- = 0$ in (10). Along this curve, p_0/p_w decreases monotonically from unity to zero as M_0 decreases from zero to $-\infty$. Therefore, $p_0/p_w = 0$ is the asymptote of curve B.

Curve C

$$\frac{p_0}{p_w} = \frac{p_{*s}/p_w}{1 + \frac{2\gamma}{\gamma+1}(\mathcal{M}^2 - 1)}, \quad M_0 = \frac{u_{*s}}{a_0} - \frac{2(\mathcal{M}^2 - 1)}{(\gamma + 1)\mathcal{M}}, \quad \mathcal{M} \geq 1, \quad (13)$$

which is obtained by letting $M_- = -1$ in (10). Along this curve, p_0/p_w decreases monotonically from p_{*s}/p_w to zero as M_0 decreases from u_{*s}/a_0 to $-\infty$. Therefore, this curve shares its asymptote $p_0/p_w = 0$ with curve B.

It should be noted that curves B and C do not intersect each other, because they are isolines for a different value of M_- .

There are a few comments on the behavior of the mixture on the boundary curves. On curve A, along which $\mathcal{M} = 1$, the shock wave is infinitesimal, so that the US_+ is identical to the undisturbed US and the US_- is directly connected to the latter. On curve B, along which $M_- = 0$, evaporation stops because $M_- = 0$ implies $u_- = 0$. On curve C, along which $M_- = 1$, the US_- is a sonic state.

In the discussions above, we did not pay attention to the relations on the temperature and concentration, i.e., the second equation of (5a), the first equation of (5b), and the second equation of (8). It is because there is no relation across the contact layer for those quantities. The relations on the temperature and concentration will be used when we need to recover the complete information about the US_{\pm} from the full set of (5)–(8). The recovery of the complete information, including the position of the shock wave in the X_1/t -coordinate, is possible because the pair of \mathcal{M} and M_- is uniquely determined for any given pair of M_0 and p_0/p_w in region I (T_0/T_w and χ_0^A are fixed). The asymptotic profile indicated by dash-dot line in Figure 1 was thus obtained.

4.1.2. Parameter range of type II

The behavior of type II is schematically shown in Figure 8, where the abbreviation EWR of the expansion wave R is introduced. The half space is divided, according to the local state of the mixture, into six parts as

$$(KL)+(US_-)+(CL)+(US_+)+(EWR)+(undisturbed\ US),$$

where the order of each part corresponds to the position from the interface with the condensed phase.

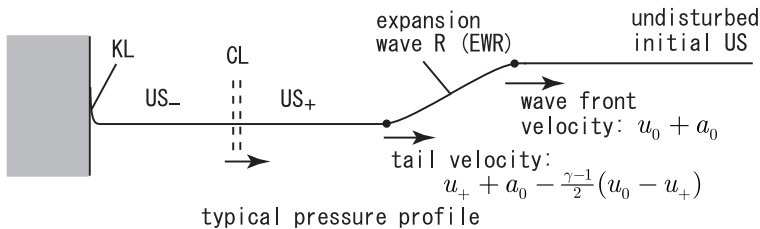


Figure 8. Schematic of the behavior of mixture: type II.

In the present case, there is a relation

$$\frac{p_+}{p_0} = \left(\frac{T_+}{T_0}\right)^{\frac{\gamma}{\gamma-1}}, \quad \frac{T_+}{T_0} = \left(1 - \frac{\gamma-1}{2} \frac{u_0 - u_+}{a_0}\right)^2, \quad \frac{\chi_+^A}{\chi_0^A} = 1, \quad (14)$$

between the undisturbed US and US_+ because of the expansion wave, while the relations (6) and (8) in Section 4.1.1 remain unchanged. The relations (14), (6), and (8) are considered under the restriction

$$0 \leq \frac{u_0 - u_+}{a_0} \leq \frac{2}{\gamma-1}, \quad u_- \geq 0, \quad (15)$$

where the former is due to the expansion wave and the latter due to the evaporation.

As in Section 4.1.1, we fix the values of T_0/T_w and χ_0^A and derive the region in the M_0 - p_0/p_w plane where the type II be observed (region II, for short). The representation of region II is readily obtained from the first and second equations of (14), the first and last equations of (8), and (6) as

$$\frac{p_0}{p_w} = h_p(M_-; \chi_w^A) \left[1 - \frac{\gamma-1}{2} \left(M_0 - \frac{a_w}{a_0} h_u(M_-; \chi_w^A)\right)\right]^{-\frac{2\gamma}{\gamma-1}}, \quad (16a)$$

where M_- is an arbitrary constant satisfying $0 \leq M_- \leq 1$ and M_0 is subject to the restriction

$$\frac{a_w}{a_0} h_u(M_-, \chi_w^A) \leq M_0 \leq \frac{a_w}{a_0} h_u(M_-, \chi_w^A) + \frac{2}{\gamma-1}. \quad (16b)$$

The region II expressed by (16) is shown in Figure 9, in which the isoline of M_- is also drawn. As is shown in the figure, it is seen from (16a) that, along each isoline of M_- , p_0/p_w monotonically increases from $h_p(M_-; \chi_w^A)$ to ∞ as M_0 increases from $\frac{a_w}{a_0} h_u(M_-; \chi_w^A)$ to $\frac{a_w}{a_0} h_u(M_-; \chi_w^A) + \frac{2}{\gamma-1}$. Therefore, $M_0 = \frac{a_w}{a_0} h_u(M_-; \chi_w^A) + \frac{2}{\gamma-1}$ is the asymptote of the isoline. It should be noted that the starting point of the isoline $(M_0, p_0/p_w) = (\frac{a_w}{a_0} h_u(M_-; \chi_w^A), h_p(M_-; \chi_w^A))$ is on curve A in Section 4.1.1. Since p_0/p_w is monotonically decreasing with respect to M_- from (16a) by Conjecture 1, region II has three boundary curves expressed as extreme cases of (16):

Curve A

the same curve as that in Section 4.1.1. This curve is obtained by letting $M_0 = \frac{a_w}{a_0} h_u(M_-; \chi_w^A)$ in (16).

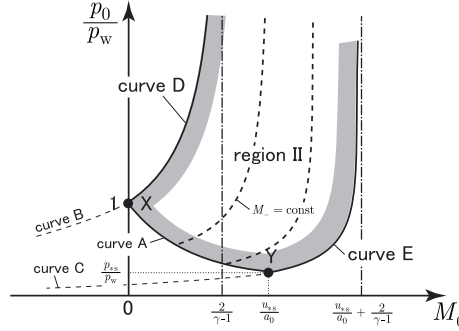


Figure 9. Schematic of region II in the M_0 - p_0/p_w plane.

Curve D

$$\frac{p_0}{p_w} = \left(1 - \frac{\gamma-1}{2} M_0\right)^{-\frac{2\gamma}{\gamma-1}}, \quad 0 \leq M_0 \leq \frac{2}{\gamma-1}, \quad (17)$$

which is obtained by letting $M_- = 0$ in (16). Along this curve, p_0/p_w takes the value of unity at point X, increases monotonically with M_0 , and tends to ∞ as $M_0 \rightarrow \frac{2}{\gamma-1}$. Therefore, $M_0 = \frac{2}{\gamma-1}$ is the asymptote of this curve.

Curve E

$$\frac{p_0}{p_w} = \frac{p_{*s}}{p_w} \left[1 - \frac{\gamma-1}{2} \left(M_0 - \frac{u_{*s}}{a_0}\right)\right]^{-\frac{2\gamma}{\gamma-1}}, \quad (18a)$$

$$\frac{u_{*s}}{a_0} \leq M_0 \leq \frac{u_{*s}}{a_0} + \frac{2}{\gamma-1}, \quad (18b)$$

which is obtained by letting $M_- = 1$ in (16). Along this curve, p_0/p_w takes the value of p_{*s}/p_w at point Y, increases monotonically with M_0 , and tends to ∞ as $M_0 \rightarrow \frac{u_{*s}}{a_0} + \frac{2}{\gamma-1}$. Therefore, $M_0 = \frac{u_{*s}}{a_0} + \frac{2}{\gamma-1}$ is the asymptote of this curve.

It should be noted that curves D and E do not intersect each other, because they are isolines for a different value of M_- . By the way, curve D meets curve B at point X, while curve E does curve C at point Y. Their connections are smooth, and each of the merged curve has a continuous third order derivative at the connection point.

There are a few comments on the behavior of the mixture on the boundary curves. On curve A, the expansion wave is infinitesimal, because $M_0 = \frac{a_w}{a_0} h_u(M_-; \chi_w^A)$ implies $u_0 = u_- = u_+$. Therefore, the US_+ is identical to the undisturbed US and the US_- is directly connected to the latter by the contact layer. This situation is the same as that in the limit from region

I to the same curve, which explains the reason for curve A to be located between regions I and II. On curve D, evaporation stops because $M_- = 0$ (thus $u_- = 0$) along the curve. On curve E, along which $M_- = 1$, the US_- is a sonic state as in the case of curve C in Section 4.1.1.

Since M_- is uniquely determined for any given pair of M_0 and p_0/p_w in region II (T_0/T_w and χ_0^A are fixed), we can recover the complete information about the US_{\pm} , including the temperature and concentration, from the full set of relations (6), (8), (14), and (15). Then it is easy to obtain the asymptotic profile indicated by dash-dot line in Figure 2.

4.1.3. Parameter range of type III

The behavior of type III is schematically shown in Figure 10, where the abbreviation EWL of the expansion wave L is introduced. The half space is divided, according to the local state of the mixture, into seven parts as

$$(KL)+(EWL)+(US_-)+(CL)+(US_+)+(SW)+(undisturbed\ US),$$

where the order of each part corresponds to the position from the interface with the condensed phase. Here, important is the fact that the tail of KL or equivalently the upstream of EWL is in a sonic (equilibrium) state. Therefore, the wave front of EWL does not move relative to the interface.

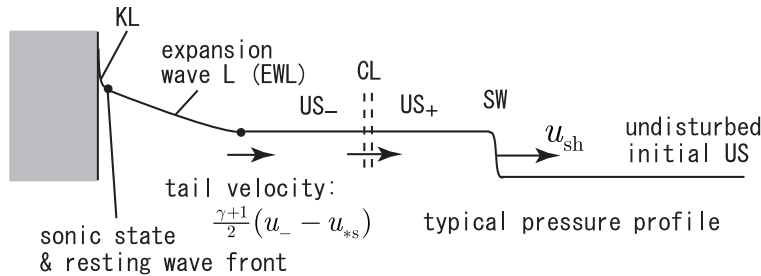


Figure 10. Schematic of the behavior of mixture: type III.

In the present case, the relations in hands are the shock relation (5), the relation across the contact layer (6), and the relation across the expansion wave L

$$\frac{p_-}{p_{*s}} = \left(\frac{T_-}{T_{*s}}\right)^{\frac{\gamma}{\gamma-1}}, \quad \frac{T_-}{T_{*s}} = \left(\frac{\gamma+1}{2} - \frac{\gamma-1}{2} \frac{u_-}{a_{*s}}\right)^2, \quad \frac{\chi_-^A}{\chi_{*s}^A} = 1, \quad (19)$$

where the quantities with subscript *s are those in the sonic state at the tail of KL [see (4)]. Note that $a_{*s} = u_{*s}$. The relations (5), (6), and (19) are subject to the restriction

$$u_+ \geq u_0, \quad \mathcal{M} \geq 1, \quad \frac{\gamma+1}{\gamma-1} u_{*s} \geq u_- \geq u_{*s} (> 0), \quad (20)$$

where the first two conditions are due to the shock wave while the last one for u_- due to the expansion wave L.

Again, we fix the values of T_0/T_w and χ_0^A and derive the region in the M_0 - p_0/p_w plane where the type III be observed (region III, for short). In the same way as in Section 4.1.1, the second and third equations of (5b) yield (9), and thus the first condition in (20) is automatically satisfied under the second condition $\mathcal{M} \geq 1$. After some manipulations, the representation of region III is obtained from the first equation of (5a), the first and second equations of (19), and (6) as

$$\frac{p_0}{p_w} = \frac{p_{*s}/p_w}{1 + \frac{2\gamma}{\gamma+1}(\mathcal{M}^2 - 1)} \left[\frac{\gamma+1}{2} - \frac{\gamma-1}{2} \left(M_0 + \frac{2(\mathcal{M}^2 - 1)}{(\gamma+1)\mathcal{M}} \right) \frac{a_0}{u_{*s}} \right]^{\frac{2\gamma}{\gamma-1}}, \quad (21a)$$

where $\mathcal{M} \geq 1$ and M_0 is subject to the restriction

$$\frac{u_{*s}}{a_0} \leq M_0 + \frac{2(\mathcal{M}^2 - 1)}{(\gamma+1)\mathcal{M}} \leq \frac{\gamma+1}{\gamma-1} \frac{u_{*s}}{a_0}. \quad (21b)$$

The region III is shown in Figure 11, in which the isoline of \mathcal{M} is also drawn. As is shown in the figure, it is seen from (21a) that, along the isoline of \mathcal{M} , p_0/p_w monotonically decreases from $\frac{p_{*s}/p_w}{1 + \frac{2\gamma}{\gamma+1}(\mathcal{M}^2 - 1)}$ to zero as M_0 increases from $\frac{u_{*s}}{a_0} - \frac{2(\mathcal{M}^2 - 1)}{(\gamma+1)\mathcal{M}}$ to $\frac{\gamma+1}{\gamma-1} \frac{u_{*s}}{a_0} - \frac{2(\mathcal{M}^2 - 1)}{(\gamma+1)\mathcal{M}}$. The isoline meets the M_0 -axis tangentially, which is readily seen by taking the derivative of (21a), and its starting point is on curve C in Section 4.1.1. Since p_0/p_w is monotonically decreasing with respect to \mathcal{M} from (21a), region III has three boundary curves expressed as extreme cases of (21):

Curve C

the same curve as that in Section 4.1.1. This curve is obtained by letting $M_0 + \frac{2(\mathcal{M}^2 - 1)}{(\gamma+1)\mathcal{M}} = \frac{u_{*s}}{a_0}$ in (21).

Half line F

$$p_0/p_w = 0, \quad M_0 \leq \frac{\gamma+1}{\gamma-1} \frac{u_{*s}}{a_0}. \quad (22)$$

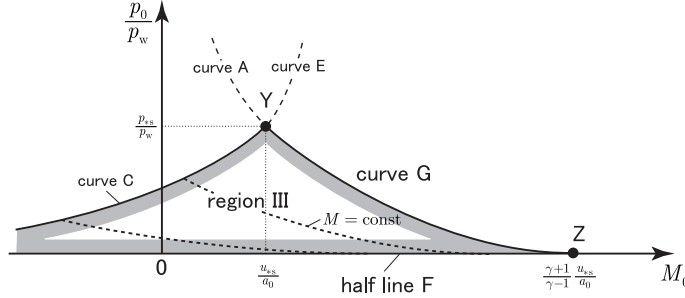


Figure 11. Schematic of region III in the M_0 - p_0/p_w plane.

This half line is obtained by letting $M_0 + \frac{2(\mathcal{M}^2-1)}{(\gamma+1)\mathcal{M}} = \frac{\gamma+1}{\gamma-1} \frac{u_{*s}}{a_0}$ in (21) and by taking into account $\mathcal{M} \geq 1$.

Curve G

$$\frac{p_0}{p_w} = \frac{p_{*s}}{p_w} \left(\frac{\gamma+1}{2} - \frac{\gamma-1}{2} \frac{a_0}{u_{*s}} M_0 \right)^{\frac{2\gamma}{\gamma-1}}, \quad (23a)$$

with

$$\frac{u_{*s}}{a_0} \leq M_0 \leq \frac{\gamma+1}{\gamma-1} \frac{u_{*s}}{a_0}, \quad (23b)$$

which is obtained by letting $\mathcal{M} = 1$ in (21).

It should be noted that curve G meets the M_0 -axis tangentially at point Z in the figure, because it is the isoline $\mathcal{M} = 1$.

There are a few comments on the behavior of the mixture on the boundary curves. On curve C, the expansion wave L is infinitesimal, because $M_0 + \frac{2(\mathcal{M}^2-1)}{(\gamma+1)\mathcal{M}} = \frac{u_{*s}}{a_0}$ implies $u_{*s} = u_-$. Therefore, the US_- is no other than the sonic state at the tail of KL. This is the same situation as that in the limit $M_- \rightarrow 1$ from region I, explaining the reason for curve C to be located between regions I and III. On curve G, along which $\mathcal{M} = 1$, the shock wave is infinitesimal and the US_+ is identical to the undisturbed US . On the half line F, the undisturbed US is the vacuum.

Since \mathcal{M} is uniquely determined for any given pair of M_0 and p_0/p_w in region III (T_0/T_w and χ_0^A are fixed), we can obtain the complete information about the US_{\pm} , including the temperature and concentration, from the full set of relations (5), (6), (19), and (20). Then it is easy to obtain the asymptotic profile indicated by dash-dot line in Figure 3.

4.1.4. Parameter range of type IV

The behavior of type IV is schematically shown in Figure 12. The half space is divided, according to the local state of the mixture, into seven parts as

$$(KL)+(EWL)+(US_-)+(CL)+(US_+)+(EWR)+(undisturbed\ US),$$

where the order of each parts corresponds to the position from the interface with the condensed phase. Here, as in Section 4.1.3, important is the fact that the tail of KL or equivalently the upstream of EWL is a sonic (equilibrium) state. Therefore, the wave front of EWL does not move relative to the interface.

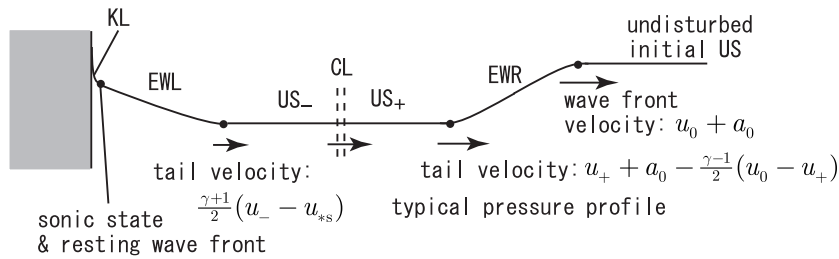


Figure 12. Schematic of the behavior of mixture: type IV.

In the present situation, the relations in hands are the relation across the expansion wave R (14), the relation across the contact layer (6), and the relation across the expansion wave L (19), where the quantities with subscript $*s$ are again those at the sonic state at the tail of KL [see (4)]. The relations (14), (6), and (19) are subject to the restriction

$$0 \leq \frac{u_0 - u_+}{a_0} \leq \frac{2}{\gamma - 1}, \quad \frac{\gamma + 1}{\gamma - 1} u_{*s} \geq u_- \geq u_{*s}, \quad (24)$$

where the former is due to the expansion wave R while the latter due to the expansion wave L.

As in the previous subsections, we fix the values of T_0/T_w and χ_0^A and derive the region in the M_0-p_0/p_w plane where the type IV be observed (region IV, for short). The procedure of deriving the representation itself is essentially just a repetition of those in the previous subsections, but the

result is the most important in the classification of evaporation to be discussed in Sections 4.1.5 and 4.2. The resulting expression of region IV is the following:

$$\frac{p_0}{p_w} = \frac{p_{*s}}{p_w} \left(\frac{\frac{\gamma+1}{2} - \frac{\gamma-1}{2} \frac{u_+}{u_{*s}}}{1 - \frac{\gamma-1}{2} \left(M_0 - \frac{u_+}{a_0} \right)} \right)^{\frac{2\gamma}{\gamma-1}}, \quad (25a)$$

where M_0 and u_+ are subject to the restriction

$$\frac{u_+}{a_0} \leq M_0 \leq \frac{2}{\gamma-1} + \frac{u_+}{a_0}, \quad u_{*s} \leq u_+ \leq \frac{\gamma+1}{\gamma-1} u_{*s}. \quad (25b)$$

The region IV is shown in Figure 13, in which the isoline of u_+ is also drawn. As is shown in the figure, it is seen from (25) that, as far as $u_+ < \frac{\gamma+1}{\gamma-1} u_{*s}$, along the isoline of u_+ , p_0/p_w monotonically increases from $(\frac{\gamma+1}{2} - \frac{\gamma-1}{2} \frac{u_+}{u_{*s}})^{\frac{2\gamma}{\gamma-1}}$ to ∞ as M_0 increases from $\frac{u_+}{a_0}$ to $\frac{u_+}{a_0} + \frac{2}{\gamma-1}$. Therefore, $M_0 = \frac{u_+}{a_0} + \frac{2}{\gamma-1}$ is the asymptote of the isoline. The starting point of the isoline $(M_0, p_0/p_w) = (\frac{u_+}{a_0}, \frac{p_{*s}}{p_w} (\frac{\gamma+1}{2} - \frac{\gamma-1}{2} \frac{u_+}{u_{*s}})^{\frac{2\gamma}{\gamma-1}})$ is on the curve G in Section 4.1.3. Since p_0/p_w is monotonically decreasing with respect to u_+ from (25), the value of u_+ is uniquely determined by the pair of $(M_0, p_0/p_w)$, and region IV has four boundary curves that are expressed as extreme cases of (25):

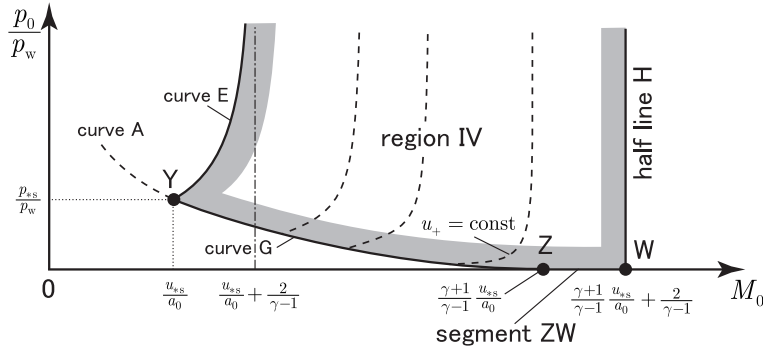


Figure 13. Schematic of region IV in the M_0 - p_0/p_w plane.

Curve E

the same curve as that in Section 4.1.2. This curve is obtained by letting $u_+ = u_{*s}$ in (25).

Curve G

the same curve as that in Section 4.1.3. This curve is obtained by letting $M_0 = \frac{u_+}{a_0}$ in (25).

Segment ZW

$$\frac{p_0}{p_w} = 0, \quad \frac{\gamma + 1}{\gamma - 1} \frac{u_{*s}}{a_0} \leq M_0 < \frac{\gamma + 1}{\gamma - 1} \frac{u_{*s}}{a_0} + \frac{2}{\gamma - 1}. \quad (26)$$

This segment is obtained by letting $u_+ = \frac{\gamma+1}{\gamma-1}u_{*s}$ in (25).

Half line H

$$\frac{p_0}{p_w} \geq 0, \quad M_0 = \frac{\gamma + 1}{\gamma - 1} \frac{u_{*s}}{a_0} + \frac{2}{\gamma - 1}. \quad (27)$$

This half line is obtained by letting $M_0 \rightarrow \frac{2}{\gamma-1} + \frac{u_+}{a_0}$ and $u_+ \rightarrow \frac{\gamma+1}{\gamma-1}u_{*s}$ simultaneously in (25). The arbitrariness of the value of p_0/p_w comes from that of the rate of the two limiting processes.³

There are a few comments on the behavior of the mixture on the boundary curves. On curve E, the expansion wave L is infinitesimal, since $u_+ = u_{*s}$ implies $u_- = u_{*s}$ from (6). Therefore, the US₋ is no other than the sonic state at the tail of KL. This is the same situation as that obtained in the limit $M_- \rightarrow 1$ from region II, explaining the reason for curve E to be located between regions II and IV. On curve G, the expansion wave R is infinitesimal, because $M_0 = \frac{u_+}{a_0}$ implies $u_0 = u_+$. Therefore, the US₊ is identical to the undisturbed US. This is the same situation as that obtained in the limit $\mathcal{M} \rightarrow 1$ from region III, explaining the reason for curve G to be located between regions III and IV. On segment ZW, the initial undisturbed US is the vacuum. On half line H, both expansion waves L and R have fully developed to make the US₋ and US₊ vacuum. This is seen from (14) and (19), because $M_0 = \frac{\gamma+1}{\gamma-1} \frac{u_{*s}}{a_0} + \frac{2}{\gamma-1}$ implies $M_0 = \frac{2}{\gamma-1} + \frac{u_+}{a_0}$ and $u_+ = \frac{\gamma+1}{\gamma-1}u_{*s}$ [see (25b)]. It is important to notice that the relation (6) across the contact layer is retained on the half line H.

Since u_+ is uniquely determined for any given pair of M_0 and p_0/p_w in region IV (T_0/T_w and χ_0^A are fixed), we can obtain the complete information about the US_±, including the temperature and concentration, from the full

³The expression (25) shows the following two facts: (i) for every fixed M_0 in the interval of $[\frac{\gamma+1}{\gamma-1} \frac{u_{*s}}{a_0}, \frac{\gamma+1}{\gamma-1} \frac{u_{*s}}{a_0} + \frac{2}{\gamma-1}]$, p_0/p_w decreases to zero as u_+ increases to $\frac{\gamma-1}{\gamma+1}u_{*s}$, (ii) for every fixed $p_0/p_w > 0$, M_0 increases to $\frac{2}{\gamma-1} + \frac{u_{*s}}{a_0}$ as u_+ increases to $\frac{\gamma-1}{\gamma+1}u_{*s}$. Therefore, as u_+ increases to $\frac{\gamma+1}{\gamma-1}u_{*s}$, the isoline of u_+ approaches the polygonal line composed of segment ZW and half line H.

set of relations (14), (6), (19), and (24). Then, it is straightforward to obtain the asymptotic profile indicated by dash-dot line in Figure 4.

4.1.5. Summary

In Section 4.1, by the use of the conventional gas-dynamic relations and the relation across the Knudsen layer for steady evaporation, we derived the expressions of regions I–IV [the equations (10), (16), (21), and (25)] in M_0 - p_0/p_w plane for fixed values of T_0/T_w and χ_0^A and showed them separately in Figures. 7, 9, 11 and 13. As shown in Figure 14, these regions are merged into one unified region, which is bounded by a single curve composed of curves B and D (curve B+D, for short) from the left, by half line H from the right, and by the M_0 -axis from the bottom. The relevant consequence of the discussions so far is that the unified region extends only up to the half line H; it never extends to infinity to the right. This result remains true even in the case of single species systems.

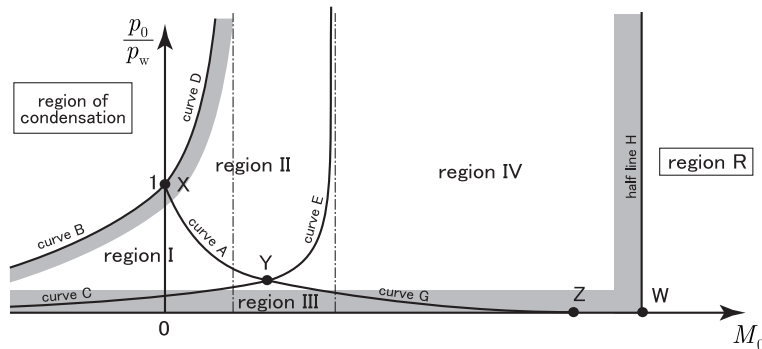


Figure 14. Schematic of regions I–IV and the remaining regions.

In order to see what happens in the region left to curve B+D, suppose that we approach this curve from the inside of the unified region. As we approach the curve, evaporation becomes weaker and weaker and finally stops on the curve because $M_- = 0$ there (see the paragraph second to the last in Sections 4.1.1 and 4.1.2); beyond the curve, the direction of flow would be reversed and condensation would occur. This situation has already been discussed and clarified in the literature with a convincing numerical evidence in the case of single species systems. Our new computations support the same conclusion for vapor mixtures (see three \square 's immediately left to curve

B+D in Figure 15). Therefore, in Figure 14, we label the region left to curve B+D as “region of condensation.” The only thing that should be newly remarked is that the boundary curve B+D, which separates the evaporation and condensation cases, is universal. That is, the curve B+D is common to any mixture of monatomic perfect gases. It is easily seen from (12) and (17).

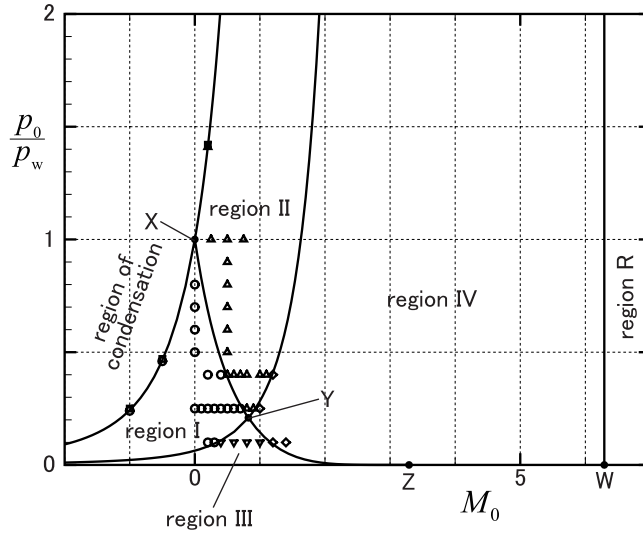


Figure 15. Classification in the M_0 - p_0/p_w plane in the case of the GSB model for $m^B/m^A = 2$, $\chi_w^A = \chi_0^A = 0.5$, $T_0/T_w = 1$. The finite-difference analysis in Section 3 was performed at the points indicated by the open symbols \circ , \triangle , ∇ , \diamond , and \square . The former four indicate the solutions of type I, II, III, and IV, whereas the latter the solution of condensation. Three pairs of neighboring points, one from the left and the other from the right to the curve B+D, are chosen to observe the behavior near the curve B+D. See also Figure 14.

On the other hand, it was not discussed in the literature about the right boundary H of the unified region. If one approaches the half line H from the left (i.e., from the region IV), the expansion waves L and R both develop to reach a critical situation where the two waves are connected by a vacuum state, as mentioned in the paragraph second to the last in Section 4.1.4. Since the critical situation is reached with retaining the relation across the contact layer, the flow velocity at the tail of expansion wave is common to L and R. As a consequence, the propagation speed of the tail of expansion

wave is common to L and R, and the vacuum region (probably a vacuum “point”) does not spread out as time goes on. Since the sonic evaporation occurs in region IV, evaporation is expected also in the region right to half line H, the “region R” in Figure 14.

The long time behavior of type I–IV described in Section 4.1 bears a resemblance to that in the piston problem in the conventional gas dynamics. In Section 4.2, we discuss the long time behavior of the mixture in region R by continuing the approach in Section 4.1. The resemblance would be helpful to understand the situation described in Section 4.2.

Incidentally, we show the classification map in the case of the GSB model in Figure 15, where the cases for which numerical computations were performed are indicated by symbols. Now, it is clear from the figure why our numerical solutions were covered by only the four-fold classification: the initial Mach number of our numerical computations were too small to go out of the right boundary of region IV. There is no contradiction between the results of numerical computations and the conventional gas-dynamic prediction.

4.2. Long time behavior in the remaining region

We now consider the long time behavior in the remaining region, right to region IV, the region R in Figure 14. The clue is the fact that a vacuum emerges between the two expansion waves L and R on the half line H. In other words, once one reaches the half line H from the left, the contact layer between two expansion waves turns into a vacuum and the two waves begin to be free from the constraint of the contact layer. The freedom from this constraint make it possible to go out of the right side boundary H.

The new type of behavior, which we induce from the behavior on half line H and call type V, is schematically shown in Figure 16. The half space is divided, according to the local state of the mixture, into five parts as,

$$(KL)+(EWL)+(Vacuum)+(EWR)+(undisturbed US),$$

where the order of each part corresponds to the position from the interface with the condensed phase. Note that, as in the case of types III and IV, the tail of KL or equivalently the upstream of EWL is in a sonic (equilibrium) state, and thus the wave front of EWL does not move relative to the interface.

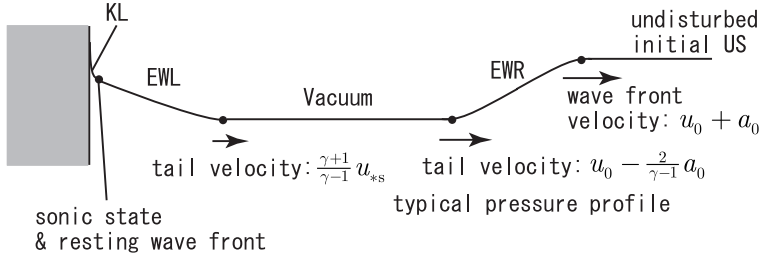


Figure 16. Schematic of the behavior of mixture: type V.

In the present case, the relations in hands are (19) with $p_-/p_{*s} = 0$ and (14) with $p_+/p_0 = 0$, because both EWL and EWR have been fully developed. These relations lead to the vanishing temperatures $T_- = T_+ = 0$ and flow velocities

$$u_- = \frac{\gamma+1}{\gamma-1} u_{*s}, \quad u_+ = \left(M_0 - \frac{2}{\gamma-1} \right) a_0, \quad (28)$$

at the tails of EWL and EWR, where subscript $-$ denotes the quantities at the tail of EWL and $+$ those at the tail of EWR. It is easy to see that u_- and u_+ in (28) are also the propagation velocity of the tail of EWL and that of EWR, respectively. Therefore, the situation considered here is possible only when the condition

$$u_{*s} \leq u_- \leq u_+ \leq u_0, \quad (29)$$

is fulfilled. Combining (28) and (29) yields the expression of the region where the new behavior of type V be observed:

$$M_0 \geq \frac{2}{\gamma-1} + \frac{\gamma+1}{\gamma-1} \frac{u_{*s}}{a_0}. \quad (30)$$

It is important to observe that the region (30), where the the behavior of type V be observed, entirely covers the remaining region, region R in Figure 14. That is, by adding type V, we can complete the classification of the long time behavior of the evaporation flow.

5. Conclusions

In the present paper, we studied the evaporation from a plane condensed phase in the case of a binary mixture of vapors on the basis of the kinetic

theory of gases, especially the long time behavior of the mixture from initial equilibrium states.

First, in Section 3, we made a summary of the existing results, especially the four-fold classification of the long time behavior, in the case of single species systems, which was induced in Ref. [10] by the conventional gas dynamics with the aid of the condition for steady evaporation (1). In the same section, we reported the results of our numerical computations for the GSB model and that they were covered by the same four-fold classification.

Next, in Section 4.1, we studied the parameter range of respective categories in the four-fold classification and describe the way of predicting the long time behavior from a give initial state by conventional gas dynamics supplemented with condition (3). The result shows that there is a region of parameters that is not covered by the four-fold classification, even in the case of single species systems. By taking as a guide the resemblance to the piston problem, we obtained a category that compensates the classification. The main feature of the category, the type V in Section 4.2, is the appearance of a vacuum between two expansion waves.

Providing a numerical evidence of type V would be desired, but we have to leave it as a future work because of the difficulty of capturing the vacuum region by the straightforward numerical computation performed in the present work. We conclude that the long time behavior of the evaporation flow is entirely covered by the five-fold classification into types I–V.

Acknowledgments

The present work is supported by the grant-in-aid for Scientific Research (No. 19560066) from JSPS and by the research grant from the UBE Foundation.

References

1. M. N. Kogan, Kinetic theory in aerothermodynamics, *Prog. Aerosp. Sci.*, **29**(1992), 271-354.
2. T. Ytrehus, Molecular-flow effects in evaporation and condensation at interfaces, *Multiphase Sci. Tech.*, **9**(1997), 205-327.
3. Y. Sone, *Kinetic Theory and Fluid Dynamics*, Birkhäuser, Boston, 2002.

4. C. Bardos, F. Golse, and Y. Sone, Half-space problems for the Boltzmann equation: A survey, *J. Statist. Phys.*, **124**(2006), 275-300.
5. Y. Sone, *Molecular Gas Dynamics*, Birkhäuser, Boston, 2007.
6. Y. Sone and Y. Onishi, Kinetic theory of evaporation and condensation – Hydrodynamic equation and slip boundary condition, *J. Phys. Soc. Jpn.*, **44**(1978), 1981-1994.
7. Y. Onishi and Y. Sone, Kinetic theory of slightly strong evaporation and condensation – Hydrodynamic equation and slip boundary condition for finite Reynolds number, *J. Phys. Soc. Jpn.*, **47**(1979), 1676-1685.
8. K. Aoki and Y. Sone, Gas flows around the condensed phase with strong evaporation or condensation – Fluid dynamic equation and its boundary condition on the interface and their application –, in *Advances in Kinetic Theory and Continuum Mechanics*, R. Gatignol and Soubbaramayer Eds., Springer, Berlin, 1991, 43-54.
9. Y. Sone, K. Aoki, and I. Yamashita, A study of unsteady strong condensation on a plane condensed phase with special interest in formation of steady profile, in *Rarefied Gas Dynamics*, V. Boffi and C. Cercignani Eds., Teubner, Stuttgart, Vol. II, 1986, 323-333.
10. Y. Sone and H. Sugimoto, Strong evaporation from a plane condensed phase, in *Adiabatic Waves in Liquid-Vapor Systems*, G. E. A. Meier and P. A. Thompson Eds., Springer, Berlin, 1990, 293-304.
11. K. Aoki, Y. Sone and T. Yamada, Numerical analysis of gas flows condensing on its plane condensed phase on the basis of kinetic theory, *Phys. Fluids A*, **2**(1990), 1867-1878.
12. K. Aoki, K. Nishino, Y. Sone and H. Sugimoto, Numerical analysis of steady flows of a gas condensing on or evaporating from its plane condensed phase on the basis of kinetic theory: Effect of gas motion along the condensed phase, *Phys. Fluids A*, **3**(1991), 2260-2275.
13. Y. Sone, Kinetic theory of evaporation and condensation: Linear and nonlinear problems, *J. Phys. Soc. Jpn.*, **45**(1978), 315-320.
14. Y. Sone, F. Golse, T. Ohwada, and T. Doi, Analytical study of transonic flows of a gas condensing onto its plane condensed phase on the basis of kinetic theory, *Eur. J. Mech. B/Fluids*, **17**(1998), 277-306.
15. C. Bardos, R. E. Caflisch, and B. Nicolaenko, The Milne and Kramers problems for the Boltzmann equation of a hard sphere gas, *Commun. Pure Appl. Math.*, **39**(1986), 323-352.
16. F. Coron, F. Golse, and C. Sulem, A classification of well-posed kinetic layer problem, *Commun. Pure Appl. Math.*, **41**(1988), 409-435.
17. S. Ukai, T. Yang, and S.-H. Yu, Nonlinear boundary layers of the Boltzmann equation I. Existence, *Commun. Pure Appl. Math.*, **236**(2003), 373-393.
18. S. Ukai, T. Yang, and S.-H. Yu, Nonlinear stability of boundary layers of the Boltzmann equation I. The case $M < 1$, *Commun. Pure Appl. Math.*, **244**(2004), 99-109.
19. K. Aoki, C. Bardos, and S. Takata, Knudsen layer for gas mixtures, *J. Statist. Phys.*, **112**(2003), 629-655.

20. S. Yasuda, S. Takata, and K. Aoki, Evaporation and condensation of a binary mixture of vapors on a plane condensed phase: Numerical analysis of the linearized Boltzmann equation, *Phys. Fluids*, **17**(2005), 047105.
21. S. Takata, Half-space problem of weak evaporation and condensation of a binary mixture of vapors, in *Rarefied Gas Dynamics*, M. Capitelli Ed., AIP, Melville, 2005, 503-508.
22. S. Takata and F. Golse, Half-space problem of the nonlinear Boltzmann equation for weak evaporation and condensation of a binary mixture of vapors, *Eur. J. Mech. B/Fluids*, **26**(2007), 105-131.
23. V. Garzó, A. Santos, and J. J. Brey, A kinetic model for a multicomponent gas, *Phys. Fluids A*, **1**(1989), 380-383.
24. P. L. Bhatnagar, E. P. Gross, and M. Krook, A model for collision processes in gases. I. Small amplitude processes in charged and neutral one-component systems, *Phys. Rev.*, **94**(1954), 511-525.
25. P. Welander, On the temperature jump in a rarefied gas, *Ark. Fys.* **7**(1954), 507-553.
26. H. W. Liepmann and A. Roshko, *Elements of Gasdynamics*, Wiley, New York, 1957.
27. A. J. Chorin and J. Marsden, *A Mathematical Introduction to Fluid Mechanics*, Third Edition, Springer-Verlag, New York, 1997.
28. R. Courant and K. O. Friedrichs, *Supersonic Flow and Shock Waves*, Wiley-Interscience, New York, 1948.
29. A. Frezzotti, Kinetic theory description of the evaporation of multi-component substances, in *Rarefied Gas Dynamics*, C. Shen Ed., Peking University Press, Beijing, 1997, 837-846.

Department of Mechanical Engineering and Science, and Advanced Research Institute of Fluid Science and Engineering, Graduate School of Engineering, Kyoto University, Kyoto 606-8501, Japan.

E-mail: takata@aero.mbox.media.kyoto-u.ac.jp